JOURNAL OF GEOPHYSICAL RESEARCH, VOL. 104, NO. D21, PAGES 26,793–26,807, NOVEMBER 20, 1999

Aerosol backscatter fraction and single scattering albedo: Measured values and uncertainties at a coastal station in the Pacific Northwest

T. L. Anderson,[1] D. S. Covert,[2] J. D. Wheeler,[2,3] J. M. Harris,[4] K. D. Perry,[5]
B. E. Trost ,[6] D. J. Jaffe,[6,7] and J. A. Ogren[4]

Abstract. Light scattering, hemispheric backscattering, and absorption properties of submicrometer and supermicrometer aerosol particles at low relative humidity and 550 nm wavelength are investigated as a function of air mass category during a 2-month campaign at a midlatitude Pacific coastal station at Cheeka Peak, Washington. The main source of uncertainty in single scattering albedo (ω) measurements, namely, the measurement of light absorption, is addressed by the deployment of three identical absorption photometers and by relying on a recent calibration of this device using direct optical measurements. The absorption photometer measurement is corrected for response to light scattering, and measurements of sea-salt aerosol in this campaign provide a partial validation of this correction. Scattering measurements by nephelometry are also corrected for known instrumental nonidealities. Uncertainties stemming from instrumental noise, drift, calibration, and correction factors are propagated to allow comparisons among air mass categories and with other data sets and, ultimately, to constrain the values of ω and other optical properties used in climate models. Marine aerosol over the midlatitude eastern Pacific is found to be weakly absorbing for the sub-μm component and virtually nonabsorbing for the super-μm component (separated at 1 μm, low-relative humidity, aerodynamic diameter). A distinct increase in sub-μm light extinction (especially absorption) observed during 2 days of sustained marine flow appears to be Asian pollution transported across the Pacific. Low levels of gaseous NO_x during this period rule out nearby combustion sources, and low levels of particulate Fe, Al, and Si rule out a significant contribution from mineral dust. Excluding this episode, both scattering and absorption properties for marine sampling conditions are similar to those observed in the clean midlatitude Southern Hemisphere (Cape Grim, Tasmania). In general, continental influence, as indicated by trends over the air mass categories, tends to raise the backscatter ratio and lower ω. Light absorption values compared to previous marine and coastal measurements confirm the range of values found by others and the highly variable nature of this quantity.

1. Introduction

For a given aerosol optical depth, top-of-atmosphere radiative forcing depends crucially on the aerosol backscatter fraction b and single scattering albedo ω [*Haywood and Shine,* 1995]. Little data exist on the latter parameter [*Hansen et al.,* 1997], and past data quality is questionable due primarily to calibration uncertainties affecting the light absorption measurement [*Heintzenberg et al.*, 1997]. Here we expand the existing data set for both b and ω with measurements characterizing the NE Pacific and the coastal region of NW Washington state. This region was notably lacking in ω data according to a recent assessment [*Liousse et al.,* 1996]. As in most previous studies, our light absorption measurements use a filter-based, differential transmission device. In accord with the recommendations of *Heintzenberg et al.* [1997], this device has been calibrated against direct optical measurements (extinction minus scattering for suspended particles), and the calibration scheme includes a correction for the response to light scattering. Other climatically relevant optical properties are also investigated, including the wavelength dependence of light scattering and the fraction of scattering and absorption attributable to sub-μm particles.

2. Methods

2.1. Sampling Site and Protocols

Measurements were made in March and April 1997, at the University of Washington Cheeka Peak Research Station (48.3°N, 124.6°W, 480 m, Figure 1). Since 1993, this station has been part of the National Oceanic and Atmospheric Administration (NOAA)/Climate Monitoring and Diagnostics Laboratory (CMDL) network of aerosol research stations. Ambient air is drawn from the top of a 10 m tower into a large vertical duct 40 cm in diameter. The central portion of this flow is drawn into a 5 cm pipe, heated by about 10°C to lower the relative humidity (RH) below 40%, and distributed

[1]Joint Institute for the Study of the Atmosphere and Ocean, University of Washington, Seattle.
[2]Department of Atmospheric Sciences, University of Washington, Seattle.
[3]Now at Oregon State University, Corvallis.
[4]Climate Monitoring and Diagnostic Laboratory, NOAA, Boulder, Colorado.
[5]Crocker Nuclear Laboratory, University of California, Davis.
[6]Department of Geophysics, University of Alaska, Fairbanks.
[7]Now at University of Washington, Bothell.

Paper number 1999JD900172.
0148-0227/99/1999JD900172$09.00

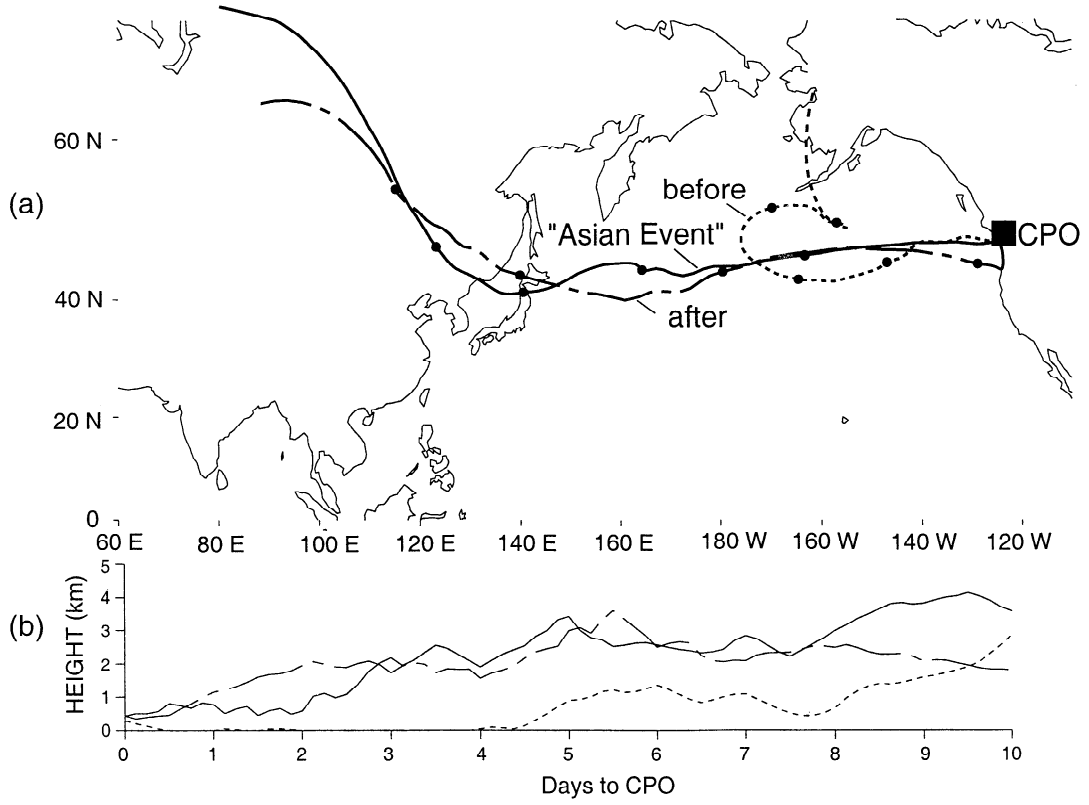

Figure 1. Cheeka Peak location and selected isentropic 10-day back trajectories surrounding the Asian pollution episode (day 87.75-89.00). The trajectory arrival times are 87.5 ("before"), 88.0 ("Asian event"), and 89.5 ("after"). Each dot represents 2 days. (a) plan view of back trajectories. (b) Vertical view of back trajectories.

to the various aerosol instruments. The spring 1997 campaign focused on measurements of light absorption using a recently developed and calibrated instrument (described below). This aerosol optics experiment coincided with a campaign focused on gas-phase oxidant chemistry. The spring was chosen because strong tropospheric transport occurring at that time optimized the use of our fixed coastal station to characterize regional-scale atmospheric phenomena.

Following standard NOAA/CMDL protocol, aerosol optical properties were studied at low relative humidity (10 < RH < 40%) and for size-segregated particles. Light scattering and hemispheric backscattering at three wavelengths were measured with an integrating nephelometer and light absorption at one wavelength was measured by differential transmission through a filter. The absorption measurement was made immediately downstream of the nephelometer, ensuring that scattering and absorption properties were measured on the identical aerosol. (Particle losses during passage through the nephelometer are negligible for sub-μm particles and are less than 10% for the super-μm particles; [*Anderson and Ogren*, 1998]). Upstream of the nephelometer, a pair of multi-orifice impactors [*Berner et al.*, 1979], with greased substrates to prevent bounce, imposed low-RH, aerodynamic cutpoints of 10 μm (always) and 1 μm (alternating). Sample air alternately passed through or around the 1 μm impactor with a 5-min switching time. The first minute of data following each switch was discarded. Using this technique, the sub-μm aerosol was measured directly, while scattering and absorption by super-μm particles must be determined by subtracting the sub-μm measurements from the sub-10 μm measurements.

2.2. Instrumentation

Light scattering and backscattering at three wavelengths were measured with an integrating nephelometer (model 3563, TSI, Inc., St. Paul, Minnesota). The design, calibration, and performance evaluation of this device are discussed by *Anderson et al.* [1996]. Field evaluation and methods of data reduction and uncertainty analysis are presented by *Anderson and Ogren* [1998].

Light absorption at one wavelength (550 nm) was measured using three absorption photometers (model PSAP, or Particle Soot Absorption Photometer; Radiance Research, Seattle, Washington). This device responds to differential light transmission through a glass fiber filter (E70-2075W, Pallflex Products Corp., Putnam, Connecticut) as particles are loaded onto the filter. The light source is a green (nominally 567 nm) light emitting diode, and the device is calibrated against a direct optical reference (extinction minus scattering). As described below, we adjust the manufacturer's calibration and estimate the instrumental uncertainty based on a recent calibration study [*Bond et al.*, 1999] that applies to the target 550 nm wavelength and includes a correction for the instrumental response to light scattering.

Size-resolved aerosol composition was monitored with 8-hour time resolution using a rotating drum impactor [*Raabe et*

al., 1988] and particle-induced X-ray emission (PIXE) analysis [*Cahill,* 1995]. Elemental concentrations (Na and heavier) were determined for particles above and below 1 μm in aerodynamic diameter (corresponding to the size segregation used in the optical measurements.) From these, mass concentrations of three aerosol components were estimated: sea-salt (using Na, Mg, Cl, and S), non-sea-salt sulfate (using S corrected for sea-salt), and dust (using Al, Si, non-sea-salt Ca, and Fe). The absolute accuracy of these component mass concentrations is questionable, especially for the dominant mass component, sea-salt, which relies largely on the most difficult element to quantify, Na. Nevertheless, the chemical data provide a valuable qualitative identification of aerosol type, and, in particular, allow us to rule out mineral dust as a significant aerosol component during the Asian event, described below. Additional information on aerosol chemistry at Cheeka Peak during marine sampling can be found in previous studies [*Quinn et al.,* 1995; *McInnes et al.,* 1996].

Standard instruments were used to monitor wind speed, wind direction, air temperature, and relative humidity (RH). The presence or absence of fog at the sample inlet was monitored by a forward scattering, near-infrared visiometer. Radon gas, which is a useful continental tracer owing to its 3.8 day half-life and exclusively continental sources, was monitored with 30-min time resolution and a detection limit of 100 mBq m^{-3} by a zinc-sulfide photomultiplier system responding to alpha particles from radon daughter products captured on a filter. (A comparable device is described by *Whittlestone et al.* [1996].) The sum of NO(g) and NO_2(g), designated NO_x, is a useful tracer of recent combustion emissions into an air parcel since it has a low background concentration (below 250 ppt) and a short atmospheric lifetime (less than 1 day). NO_x was measured with 6-min time resolution by a high-sensitivity chemiluminescent instrument [*Beine et al.*, 1997].

2.3. Air Mass Categories

Air mass categories were assigned to each hourly average using meteorological and back trajectory information. Aerosol optical data were not considered except, as discussed below, in separating the highly unusual Asian event from the rest of the marine air mass samples. Back trajectories use the model described by *Harris and Kahl* [1994] and data from the European Centre for Medium-Range Weather Forecasts. This is an isentropic model except within 100 m of the surface where air parcels are advected by the mean 100 to 600 m winds. Example trajectories are shown in Figure 1.

The defining criteria and frequency of occurrence of each air mass category are shown in Table 1. In all, 1279 hours of valid aerosol data were obtained during the 2-month campaign. From this, we exclude hours when fog (i.e., cloud at the level of the aerosol inlet) is present more than 20% of the time, since the inlet efficiency is known to be significantly less than unity for fog droplets. In addition, samples with wind speeds below 2 m s^{-1} are removed to help avoid local contamination. The remaining 859 hours were then assigned to one of four air mass categories or to an unclassified (mostly transitional) category. In all, 661 hours were classified and analyzed.

The "marine" category is intended to characterize the existing aerosol over the midlatitude, eastern Pacific Ocean (not necessarily pristine). To do this, we required local wind direction to be between 150° and 330° and that the back trajectories show no land contact (other than the immediate coastal plain) for at least 3 days prior to sampling. Similarly, samples were classified "NA continental" (where "NA" refers to North America) if local wind direction was easterly (between 30° and 150°) and back trajectories indicated the air had been over North American land for most of the prior 3 days. An intermediate category, "NA-modified marine," was used for any wind direction when the back trajectories indicated significant land contact during the prior 3 days yet with most of that time spent over the ocean. Finally, we removed a singular episode, dubbed the "Asian-modified marine event," from the marine category for separate analysis. This was an episode of approximately 30 hours duration, during which unusually high values of many particulate and gas parameters were observed and back trajectories (Figure 1) indicated rapid trans-Pacific transport. (See *Jaffe et al.* [1999] for further discussion of this event.) The averages and standard deviations of several tracer parameters are shown in Table 1 for each of the four air mass categories.

2.4. Data Reduction

2.4.1. Overview. We report a suite of low-RH optical properties for sub- and super-μm particles at 550 nm wavelength, focusing on single scattering albedo and its uncertainty. The relevant components of light extinction by particles are total scattering σ_s, hemispheric (i.e., 90°-180°) backscattering σ_{bs}, and absorption, σ_a, all with units herein of Mm^{-1} (1 Mm = 10^6 m). (The light extinction coefficient is the space rate of direct-beam attenuation or, equivalently, the optical depth per unit length.) These are converted to the dimensionless, intensive aerosol optical properties of backscattering ratio b, Ångström exponent å, single scattering albedo ω, and sub-μm scattering fraction f, defined as follows:

$$b = \frac{\sigma_{bs}}{\sigma_s} \tag{1}$$

$$\mathring{a} = -\frac{\log\left(\sigma_s^{450}/\sigma_s^{700}\right)}{\log(450/700)} \tag{2}$$

$$\omega = \frac{\sigma_s}{\sigma_s + \sigma_a} \tag{3}$$

$$f = \frac{\sigma_s(D_{\text{aero}} < 1\mu\text{m})}{\sigma_s(D_{\text{aero}} < 10\mu\text{m})} \tag{4}$$

where b, ω, and f are referenced to 550 nm wavelength and the superscripts in (2) refer to the other wavelengths measured by the nephelometer. (An *extensive* aerosol property depends upon the amount of particulate material present per unit volume of air, while an *intensive* property does not.)

The raw data are 5-min averages of alternating sub-1 μm and sub-10 μm extinction. These data were initially reduced to 1-hour averages to allow a robust calculation of super-μm extinction, obtained by difference. After screening for fog and low wind speed and separating into air mass categories (see above), the arithmetic average, standard deviation, and uncertainty of each optical property were calculated for each air mass type. For intensive aerosol properties, we calculate extinction-weighted estimates of the average and standard deviation since this is both more robust mathematically (when values are frequently near the detection limit) and more directly relevant to climatic effects. The average and standard deviation of the backscatter ratio b, and s.d.(b), respectively,

Table 1. Criteria, Frequencies, and Characteristics of Air Mass Categories

Defining Criteria and Sampling Frequencies

Category(*)	Criteria	Number Hours	Portion of "All," %	Portion of "Dry," %	Number Events(†)
All	optical instruments working	1279			
Dry	fog present < 20% of hour WS > 2 m s^{-1}	859	67		
Marine(‡)	150°< WD < 330° 3-day back trajectory entirely over ocean	333	26	39	18
Asian-modified marine event	same as marine but with rapid trans-Pacific back trajectory and unusual aerosol characteristics	18	1.4	2.1	1
NA-modificd marinc	any wind direction 3-day back trajectory mostly over ocean but including some land contact	204	16	24	11
NA continental	30° < WD < 150° 3-day back trajectory mostly over land	106	8	12	6
Unclassified		198	15	23	

Meteorological and Airmass Tracer Characteristics(§)

Category(*)	Wind Speed,	Wind Direction,	T,	RH Ambient,(‖)	RH Nephelometer(¶)	Rn,	NO_X,	CPC,
	m s^{-1}	deg	°C	%	%	mBq m^{-3}	ppt	cm^{-3}
Marine(‡)	4.1	229	6	95	26	554	151	477
	(2.7)	(37)	(3)	(7)	(5)	(202)	(223)	(373)
Asian event	4.0	219	7	97	24	1135	101	702
	(0.7)	(25)	(2)	(4)	(0)	(100)	(44)	(144)
NA-modified marine	4.7	166	5	83	23	1010	923	1674
	(3.0)	(84)	(2)	(15)	(5)	(387)	(1127)	(1369)
NA continental	4.7	77	8	68	18	1498	1920	3698
	(3.7)	(9)	(2)	(26)	(7)	(531)	(1205)	(1253)

*NA, North America.

†Temporally separated meteorological episodes.

‡Excluding the Asian-modified marine event.

§Arithmetic averages of hourly data (standard deviations of hourly data).

‖Ambient relative humidity is exaggerated due to slow recovery of sensor from fog saturation.

¶Measured relative humidity inside the nephelometer sensing volume.

for n hourly averaged samples will illustrate this procedure:

$$\bar{b} = \frac{1}{n}\sum_{i=1}^{n}\left[b_i\sigma_{s,i}\right]\left(\overline{\sigma_s}\right)^{-1} = \overline{\sigma_{bs}} \Big/ \sigma_s \tag{5}$$

$$\text{s.d.}(b) = \left(\overline{\sigma_s}\right)^{-1}\sqrt{\frac{1}{(n-1)}\sum_{i=1}^{n}\left[\left(b_i - \bar{b}\right)\sigma_{s,i}\right]^2} \tag{6}$$

2.4.2. Adjustment and uncertainty of optical data. Scattering measurements are corrected for the angular nonidealities of the nephelometer (following *Anderson and Ogren* [1998]), which cause particle scattering in the near-forward direction to be underestimated. Wavelength nonidealities are minor by comparison [*Anderson et al.*, 1996] and are neglected. Absorption measurements are corrected based on a recent laboratory calibration [*Bond et al.*, 1999] that includes a correction factor for the absorption photometer response to light scattering. This scattering correction has a large effect on σ_a at high values of ω (as herein).

Sources of uncertainty (estimated 95% confidence levels) were quantified for each optical measurement and the derived intensives. These are listed in Table 2. Two summary statistics are reported: precision uncertainty and total uncertainty (or overall accuracy.)

Precision uncertainty $\delta\sigma_{prec}$ is calculated as

$$\delta\sigma_{prec}{}^2 = \delta\sigma_{noise}{}^2 + \delta\sigma_{drift}{}^2 \tag{7}$$

where the symbol "δ" before a variable is used to denote un-

Table 2. Optical Data Adjustments and Uncertainties

Source	Correction	Uncertainty, Mm^{-1}	Basis and Notes
		Nephelometer	
Noise	---	$f(\tau,\sigma_s)$	
Drift offset			
σ_s	see AO98	0.18	Uncertainties are calculated from repeated measurements of calibration gases during the field campaign; τ refers to sample time; corrections for drift offset and drift slope are already incorporated into σ_{sm} (see AO98 for details).
σ_{bs}	see AO98	0.10	
Drift slope			
σ_s	see AO98	$0.014*\sigma_{sm}$	
σ_{bs}	see AO98	$0.01*\sigma_{sm}$	
Calibration	---	$0.07*\sigma_s$	Laboratory closure tests (A96).
Angular nonidealities	see equation (10) and Table 3	$U_{s,ang}*\sigma_{sm}$ (see Table 3)	Mie calculations using measured angular sensitivities (A96) and a range of size distributions and refractive indices (see AO98).
		PSAP	
Noise			Drift corrections cannot be made with the PSAP because repeat calibrations in the field were not made. Drift and noise uncertainties were derived from measurements with three PSAPs operated in parallel (see text). Noise is assumed to scale with the square root of sample time, τ; τ_0 is 30 min (i.e., 1-hour time resolution). Noise for super-μm σ_a (obtained by difference) is assumed to be larger by the square root of 2.
sub-μm	---	$0.18\sqrt{\tau_0/\tau}$	
super-μm	---	$0.25\sqrt{\tau_0/\tau}$	
Drift slope			
sub-μm	---	$0.06*\sigma_{am}$	
super-μm	---	$0.06*\sigma_{am}$	
Calibration	0.820 see equation (11)	$0.20*\sigma_a$	Direct optical calibration using extinction minus scattering on suspended particles for reference absorption (B99). Note that 20% uncertainty is the estimated lower limit and is not well constrained.
Scattering response	$0.02*\sigma_{sm}$ see equation (11)	$0.01*\sigma_{sm}$	Laboratory measurements of nonabsorbing salts (B99); confirmed by sea-salt data herein (Figure 3).

Uncertainties intended as 95% confidence limits. References: AO98 is *Anderson and Ogren* [1998]; A96 is *Anderson et al.* [1996]; B99 is *Bond et al.* [1999].

certainty in that variable, and $\delta\sigma_{noise}$ and $\delta\sigma_{drift}$ are noise and drift uncertainty, respectively. As pointed out by *Anderson and Ogren* [1998], the value of computing $\delta\sigma_{prec}$ is that it allows measurements using the same instruments and protocols, but separated in space or time, to be statistically compared. In the present work, it allows statistical comparison of optical properties among air mass categories and with similar measurements at Cape Grim, Tasmania.

Total uncertainty $\delta\sigma_{total}$ is calculated as

$$\delta\sigma_{total}^2 = \delta\sigma_{prec}^2 + \delta\sigma_{cal}^2 + \delta\sigma_{corr}^2 \quad (8)$$

where $\delta\sigma_{cal}$ is the intrinsic uncertainty due to the calibration method and $\delta\sigma_{corr}$ is the uncertainty associated with corrections for known instrumental nonidealities. The value of $\delta\sigma_{total}$ is that it allows statistical comparisons with other measurement methods and quantifies the degree to which the measurements constrain acrosol optical properties used in radiative transfer models.

The scattering coefficient σ_s (and, equivalently σ_{bs}), is estimated as

$$\sigma_s = \sigma_{sm} C_{s,ang} \quad (9)$$

where σ_{sm} is the nephelometer measurement after adjustment for multiple measurements of the calibration gases (air and CO_2) during the campaign and $C_{s,ang}$ is the correction factor for nephelometer angular nonidealities. *Anderson and Ogren* [1998] present data on $C_{s,ang}$ and show that, in the case of sub-μm scattering, it can be estimated from the wavelength dependence of light scattering, as measured by the nephelometer. (A similar methodology was suggested by *Rosen et al.*, [1997].) Following *Anderson and Ogren* [1998], we estimate $C_{s,ang}$ using

$$C_{s,ang} = A_1 + A_2 \text{å} \quad (10)$$

where å is the measured Ångström exponent [equation (2)] and values of the coefficients A_1 and A_2 are given in Table 3.

The nephelometer calibration uncertainty (which applies to σ_{sm}) is set to ±7% based on laboratory closure experiments reported by *Anderson et al.* [1996]. The dimensionless uncertainties of the nephelometer angular correction factors, $U_{s,ang}$, are given in Table 3 based on Mie calculations by *Anderson and Ogren* [1998]. Repeated measurements of the calibration gases during the campaign allowed a quantification of calibration drift (slope and offset) as well as instrumental noise, as described by *Anderson and Ogren* [1998].

Table 3. Nephelometer Angular Correction Factor: Coefficients and Uncertainties

	Coefficients for Use in equation (10)		Uncertainty
	A_1	A_2	$U_{s,ang}$
sub-μm σ_s	1.152	-0.044	0.022
sub-μm σ_{bs}	0.947	0	0.009
super-μm σ_s	1.51	0	0.28
super-μm σ_{bs}	1.026	0	0.047

See *Anderson and Ogren* [1998] for further details.

Following *Bond et al.* [1999], we estimate the absorption coefficient σ_a as

$$\sigma_a = (\sigma_{am} - C_{a,scat}\sigma_{sm})C_{a,cal} \quad (11)$$

where σ_{am} is the absorption photometer measurement after flow rate and spot area adjustments [see equation (12)], $C_{a,scat}$ is a correction factor accounting for the response to scattering (set to 0.02 ±0.01), σ_{sm} is the adjusted nephelometer measurement as in (9) (that is, prior to applying the angular correction factor), and $C_{a,cal}$ is a calibration correction factor (set to 0.820).

Unlike the nephelometer, the absorption photometer cannot be calibrated routinely in the field, since this is a difficult laboratory procedure requiring a particle generation facility and instrumentation for accurate measurements of both scattering and total extinction (see *Bond et al.* [1999] for detailed description). The most obvious and easily correctable dangers associated with relying on the manufacturer's calibration involve drift in the built-in flowmeter and unit-to-unit variations in spot size. The procedure we adopt is to measure both the sample flow rate (with a bubble flowmeter) and spot area (by measuring spot diameter on several filters) and correct the raw data as follows:

$$\sigma_{am} = \sigma_{PSAP}\frac{F_{PSAP}}{F_{meas}}\left(\frac{D_{meas}}{5.1\,mm}\right)^2 \quad (12)$$

where σ_{PSAP} and F_{PSAP} are the absorption coefficient and flow rate reported by the instrument, F_{meas} and D_{meas} are the measured flow rate and spot diameter, and 5.1 mm is the spot diameter produced by the standard instrument used in the manufacturer's calibration. The flow adjustment references the measurements from all three PSAP units to the pressure and temperature inside the instrument container, which were 957 mbar and 22°C on average. Flow and spot-area correction factors differed by as much as 20% between units; however, once these adjustments were made, unit-to-unit discrepancies averaged over the campaign were found to be within 6%.

Laboratory tests with nonabsorbing aerosols (ammonium sulfate and sodium chloride) show conclusively that the absorption photometer responds to scattering. *Bond et al.* [1999] found this response to diminish as the filter is loaded with scattering particles and to increase as the filter is loaded with absorbing particles. Thus an exact correction factor cannot be established. (In principle, this would require knowledge of filter-loading history.) However, for a broad range of conditions, *Bond et al.* [1999] found that $C_{a,scat}$ can be set to 0.02 with an uncertainty of ±0.01.

As shown in (11), we also apply a calibration correction factor $C_{a,cal}$ to the PSAP. The value of $C_{a,cal}$ was found by *Bond et al.* [1999] to be 0.820 with an uncertainty for that data set of ±7%. Additional unquantified uncertainty is associated with possible systematic errors in calibration method (e.g., residual errors in wavelength or angular adjustments) and with the potentially different response of the PSAP to atmospheric particles as opposed to the test aerosol (ammonium sulfate mixed with nigrosin). *Bond et al.* [1999] suggest that the overall calibration uncertainty of the PSAP is at least ±20%. We adopt this uncertainty value herein, but point out that it is not well constrained by empirical tests.

A comparison of three identical PSAPs operated in parallel over most of the campaign was used to determine precision uncertainty. This quantity incorporates uncertainties in the flow and spot-area adjustment factors, since these were determined independently for each unit. Hourly averaged relative discrepancies (difference divided by mean) between simultaneously measuring instruments were calculated whenever both measurements were larger than 0.2 Mm^{-1}. Unlike the nephelometer, there is no offset term in the PSAP calibration; therefore the only component of drift uncertainty is the slope term. A regression of all data was used to establish a 95% confidence drift-slope uncertainty of 6%. The relative precision uncertainty is then

$$\frac{\delta\sigma_{a,prec}}{\sigma_a} = \sqrt{\left(\frac{\delta\sigma_{a,noise}}{\sigma_a}\right)^2 + 0.06^2} \quad (13)$$

Noise uncertainty, $\delta\sigma_{a,noise}$, was set to a level such that exactly 95% of the measured relative discrepancies were within the precision uncertainty calculated by (13). For hourly time resolution, the PSAP noise level determined by this method is 0.18 Mm^{-1}. (The actual sample time involved with this hourly time resolution is 24 min, corresponding to six, 5-min periods for each of the two size cuts, with the first minute of data discarded.) This applies to raw data for either the sub-μm or sub-10-μm measurements. For corrected data, the noise estimate must be multiplied by $C_{a,cal}$ from (11) (that is, by 0.820.) Noise for the super-μm measurements is assumed to be larger by $\sqrt{2}$, that is, 0.25 Mm^{-1} for raw data at hourly time resolution. For longer averaging times, noise is assumed to diminish with the square root of sample time. The calculated precision uncertainty for sub-μm σ_a is plotted in Figure 2 along with the actual hourly discrepancy measurements from the campaign.

An alternate method of estimating PSAP noise would be to make extended measurements of filtered, particle-free air. Only limited data of this type were acquired. However, during one 20-hour, foggy period, measured particle concentrations according the nephelometer were so low (σ_s = 0.07 ± 0.04 Mm^{-1}) as to be virtually equivalent to filtered air. The standard deviation of measured, hourly averaged σ_{am} over this period was 0.05 Mm^{-1} for sub-μm and 0.10 Mm^{-1} for super-μm particles. The noise levels determined from the discrepancy data (above) correspond to 3.6 and 2.5 times these standard deviations, respectively. For well-behaved, randomly distributed noise, one would expect that 2 times the standard deviation would correspond to 95% confidence. Data from this extremely clean period also revealed large unit-to-unit differences (roughly a factor of 3) in terms of the standard deviations of hourly averaged σ_{am}. We conclude that further studies of PSAP noise would be useful.

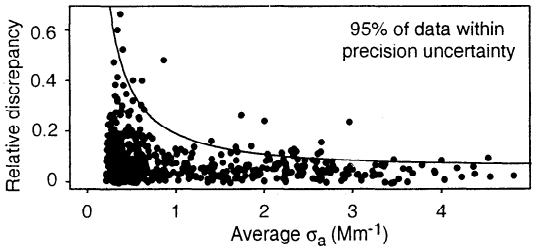

Figure 2. Empirical determination of PSAP precision uncertainty. For paired units, sampling in parallel, the relative discrepancy is plotted against the average measured absorption. Precision uncertainty (curved line) was determined from equation (13) by selecting a noise level such that exactly 95% of the data is below the line. Data are hourly averages over the 2-month campaign, using both sub-1-μm and sub-10-μm measurements.

3. Results

3.1. Absorption Validation and Uncertainty

Optical measurements of the super-μm aerosol at our coastal station provide a partial test of the scattering correction to σ_a. If we assume that, for some significant fraction of the time, the super-μm aerosol consists of pure sea salt, then our data set includes a large number of cases for which super-μm scattering is high and the true value super-μm absorption is zero. To test whether the scattering correction factor was too large, we extracted a subset of the super-μm data which had large scattering (σ_s > 10 Mm^{-1}) and very low absorption (σ_a < 0.3 Mm^{-1}). For these data, absorption uncertainty $\delta\sigma_a$ is compared to σ_a. Uncertainty in this case does not include the uncertainty in the scattering correction factor and is dominated by noise (0.25 Mm^{-1} for corrected super-μm data at hourly time resolution.) Results are shown in Figure 3 (circles). Fewer than 3% of the points are negative by an amount larger than the uncertainty. (Such points lie to the left of the dashed -1:1 line.)

Examination of the raw data (triangles) shows that the negative values are not primarily caused by the scattering correction, but rather by instrumental uncertainties. That is, these points were already negative in the raw data. For the bulk of the data, the scattering correction tends to tighten up the distribution of σ_a values and move it toward, but not below, zero. If the super-μm samples measured here were mostly uncontaminated sea salt (i.e., nonabsorbing), then this data indicate that the scattering correction of 0.02 should be, if anything, a bit larger. This is somewhat contrary to the laboratory measurements by *Bond et al.* [1999], which indicate that the scattering correction for super-μm particles might be smaller than 0.02, perhaps as small as 0.01. Overall, the uncertainty range used herein (0.01 to 0.03) seems appropriate.

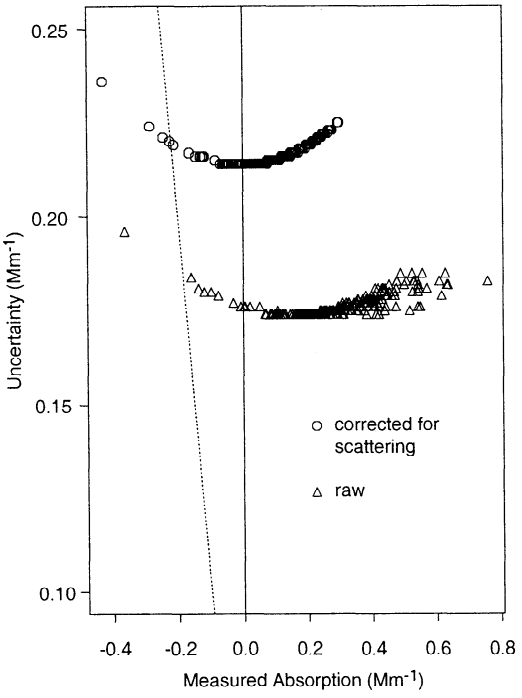

Figure 3. Test of the scattering correction to the absorption measurement. Absorption versus absorption uncertainty (estimated 95% confidence; excludes uncertainty in the scattering correction factor) for super-μm particles for hourly averaged samples with large scattering (σ_s > 10 Mm^{-1}) and very low absorption (σ_a < 0.3 Mm^{-1}). Points to the left of the diagonal line are negative by an amount larger than the estimated uncertainty. Circles, corrected absorption values σ_a. Triangles, raw absorption values σ_{am} (i.e., prior to the scattering correction). Triangles are offset on the *y* axis by -0.04 for clarity.

3.2. Asian Pollution Episode

Toward the end of day 87, during sustained westerly winds, several independent parameters indicated a dramatic change in air mass. The event lasting from this time (approximately day 87.75 UTC) until the transition to easterly winds at about 89.00 has been removed from the Marine air mass category for separate analysis in recognition of its highly distinct qualities. On the basis of the back trajectories which indicate rapid trans-Pacific transport (Figure 1), as well as other evidence discussed below (and in more detail by *Jaffe et al.* [1999]), we designate this as an "Asian" sampling event. Figure 4, which shows the optical properties of this event in the context of the rest of the marine air mass samples, demonstrates what a dramatic outlier it is, particularly in terms of sub-μm σ_a. The high value of σ_a indicates the presence of black carbon. (Our analysis eliminates both scattering artifact and mineral dust as explanations for the high σ_a.) Black carbon, in turn, indicates a combustion source, which could be Asian pollution or local contamination. The latter is virtually

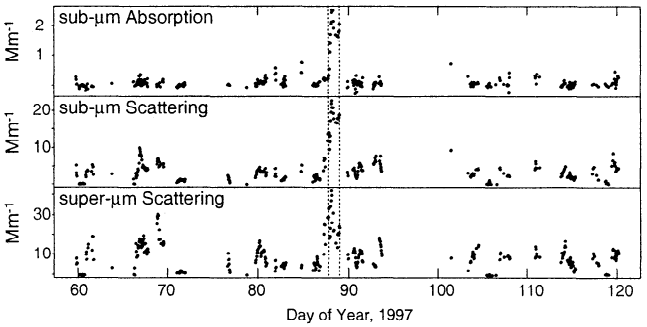

Figure 4. Asian episode in the context of all marine air mass samples. The vertical dotted lines show the estimated time boundaries of the Asian event (day 87.75 to 89.00).

ruled out, however, by the extremely low levels of NO_x (Table 1 and Figure 5). These provide clear evidence of long-range transport over the ocean.

Figure 5 shows a 4-day time series of several parameters, centered on the Asian event, which is bounded by vertical lines. The gaps in the scattering and absorption measurements are mostly caused by data exclusion whenever fog is present at the aerosol inlet. However, the gap surrounding time 87.0 was due to instrument calibration/maintenance. The Asian event was preceded by foggy, clean marine air and followed by polluted continental air from the nearby Puget Sound region. Both the condensation particle count (CPC) and radon (Rn) signals show definite (though not quite simultaneous) increases at the onset of the Asian event. Neither reaches normal continental levels, which is consistent with significant loss of Rn by radioactive decay and loss of CPC by coagulation during the 6 to 7 day transport across the Pacific. This transport time would be sufficient to completely eliminate any Asian-derived NO_x, however; and, accordingly, NO_x remains at low, clean marine levels until the transition (at day 89.0) to a North American continental air mass. Particle composition, indicated by PIXE elemental analysis, reveals that sea salt is a major constituent of both sub-μm and super-μm mass, non-sea-salt-sulfate is a major constituent of sub-μm mass, and mineral dust is not a significant mass constituent.

Thus the elevated sub-μm scattering and absorption during this event are consistent with it being an episode of Asian pollution. The combustion source is most likely industrial,

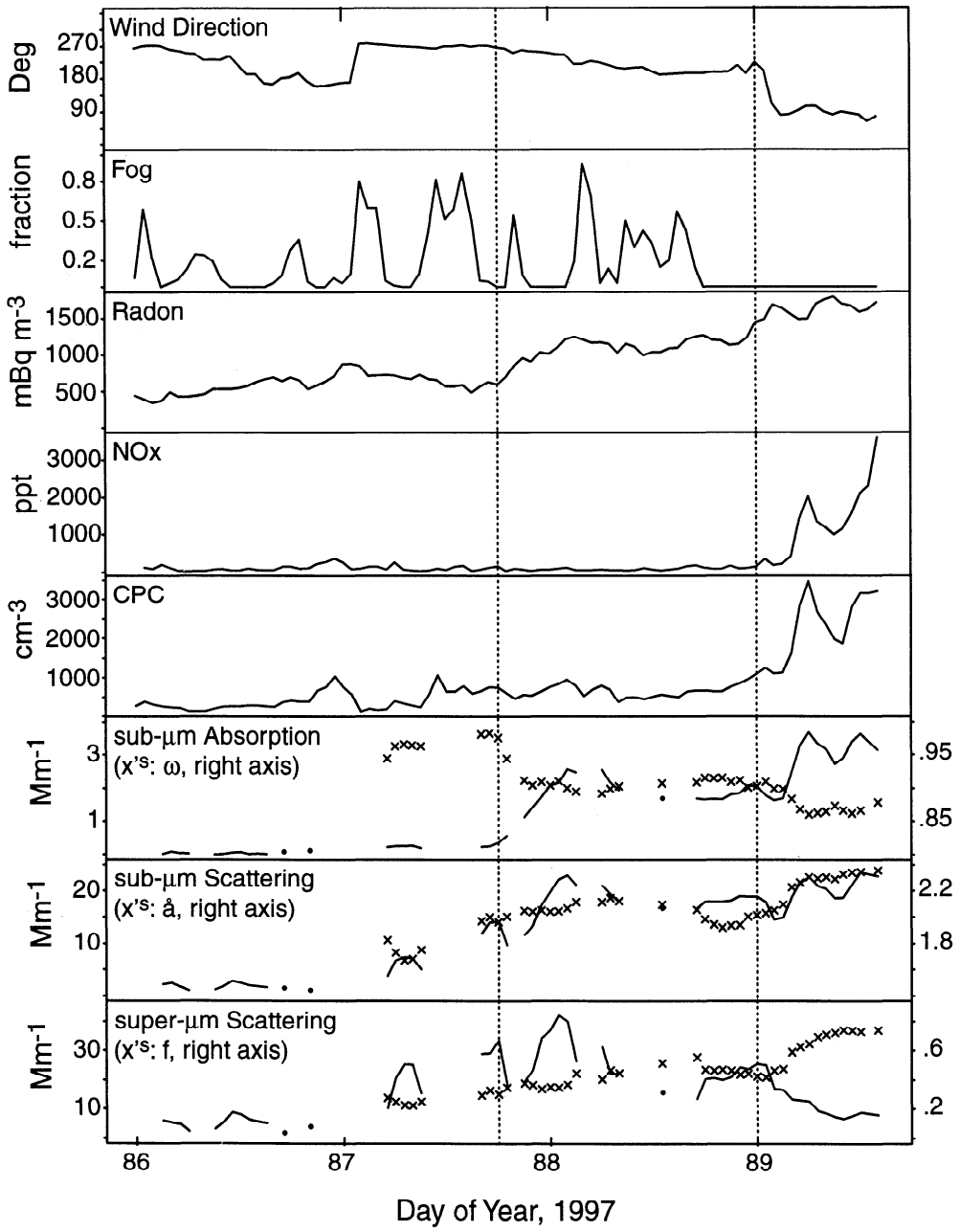

Figure 5. Meteorology, air mass tracers, and aerosol optics for 5 days centered on the Asian event. Vertical dotted lines are as in Figure 4. Bottom three panels show intensive properties with crosses: single scatter albedo ω, Ångström exponent å, and sub-μm fraction of scattering *f*, respectively.

since late March is too early for biomass burning over the East Asian boreal forests. On the other hand, the levels of sea salt and super-μm scattering, which were also unusually high in comparison to normal marine values, require a different explanation. The back trajectories indicate a long fetch over the ocean, fairly near the surface, and at high wind speeds. This is consistent with ocean buoy data for the same period. Evidently, the unusual transport event was coupled with unusually effective sea-salt production.

3.3. Optical Properties as a Function of Air Mass Type

Optical properties show significant variations among air mass categories, as shown in Table 4. Marine air masses show a dominant super-μm component (sea salt) and little absorption. Continental influence (North American or Asian) is associated with increases in sub-μm extinction, increases in the fraction of scattering due to sub-μm particles f, and decreases in sub-μm single scattering albedo ω. In addition, there is an apparent increase in backscatter fraction b for the continentally influenced air masses, although the differences in b are within the precision uncertainty and therefore not significant to 95% confidence. While the Asian event is unusual in terms of its extensive properties (σ_a and σ_s), the intensive properties, especially single scattering albedo, are similar to those associated with North American aerosol.

For both the modified marine categories and the continental category, a distinct difference in single scattering albedo ω was observed between the sub- and super-μm particles. Indeed, we observe a virtual absence of absorption by super-μm particles. These results show that a cut size of 1 μm, low-RH, aerodynamic diameter effectively separates the aerosol at our station into two size categories that are independent in terms of their absorption properties. A larger cut size (e.g., the commonly used 2.5 μm diameter separation point) would have produced a less effective separation by mixing much of the nonabsorbing category into the partially absorbing category. The high value of ω (0.99) for the super-μm aerosol during the Asian event is further evidence that the large particles are sea salt and not mineral dust.

4. Discussion

4.1. Data Quality and Uses

As described in section 2.2, aerosol chemical measurements in this study were limited to elemental analysis by PIXE for sub- and super-μm particles, with 8-hour time resolution. The information on aerosol chemistry from PIXE is largely qualitative, but is important in that it allows us to rule out mineral dust as a significant mass constituent during the Asian event. Previous studies provide information on the ionic composition of the aerosol at Cheeka Peak during marine sampling conditions [*Quinn et al.*, 1995; *McInnes et al.*, 1996].

The standard deviations shown in Table 4 provide an estimate of variability within each air mass type. Because of the short duration of the measurement campaign (2 months), these estimates must be regarded as preliminary. Year-round data for several years would be more appropriate for this purpose. Nevertheless, the data show the highly variable nature of aerosol extensive properties (σ_a and σ_s) and the less variable nature of the intensive properties.

It is worth noting the importance of the instrumental corrections to both scattering and absorption [equations (9) and (11)]. The effect of these corrections is systematic: total scatter increases (by a few percent for the sub-μm particles and 51% for super-μm), and absorption decreases (sometimes to zero). Thus the corrections have the effect of decreasing the backscatter ratio and increasing the single scattering albedo. Since many previous studies have not incorporated these corrections, comparisons should be made carefully. To facilitate this, Table 4 shows the net correction factor for each reported value. These correction factors are calculated as y/x, where y is the displayed (corrected) value of the average and x is the uncorrected value. An exception occurs in the case of the Ångström exponent (which is in log units). For this case only, the correction factor is calculated as y-x.

Uncertainty data in Table 4 show that key aerosol properties can be constrained fairly tightly by the measurement methods used herein. In general, precision uncertainty is much lower than total uncertainty, meaning that differences between air masses, between stations, and over time can be detected much more easily than can discrepancies with alternate measurement methods or with model-generated optical properties. For the backscatter ratio, a large source of uncertainty comes from the calibration offset term for backscatter. This uncertainty could be reduced by more frequent measurements of particle-free air. For single scattering albedo, uncertainty associated with the absorption measurement is dominant. The 20% calibration uncertainty assumed herein needs to be verified, and further studies of instrumental noise for the PSAP would also be in order.

The overall average of any aerosol property at our coastal station would clearly be governed by the frequency of sampling the various air mass types, since their properties are so distinct. Seasonal patterns, year-to-year trends, and multiyear averages would be affected (if not dominated) by the meteorological factors controlling these sampling frequencies, rather than by variations in aerosol sources or sinks. Thus it is much more useful to analyze, as herein, the properties of each air mass type. The validity of comparisons with chemical transport models (CTMs) is enhanced by such analysis, although care must be taken. We intend our data to be used, not as point measurements, but as providing regionally representative data for three different regions in the vicinity of our station: the NE Pacific (marine category), coastal (NA-modified marine), and NW North America (continental). In addition to permitting regional comparisons, the 1997 field campaign included a distinct long-range transport event (the Asian-modified marine event) that could be used to assess transport efficiency and variability within CTMs.

4.2. Comparison to Other Data Sets

Our scattering data can be directly compared to springtime measurements at the Southern Hemisphere, midlatitude, coastal station of Cape Grim, Tasmania (40.7°S, 144.6°E, 104 m). Comparable data were acquired at Cape Grim during the First Aerosol Characterization Experiment (ACE 1) from November 15 to December 15, 1995 [*Carrico et al.*, 1998]. Measurements during marine-sector sampling at Cape Grim are compared to the Cheeka Peak marine air mass category in Table 5. On the basis of the use of identical nephelometers and sampling protocols, we apply the same correction scheme to the Cape Grim scattering data as that used herein (see col-

Table 4. Optical Measurements for Each Air Mass Type

	σ_a (Mm^{-1})	σ_s (Mm^{-1})	å	*b*	ω	*f*
			Marine (Excluding Asian Event)			
Sub - µm						
average	0.09	3.34	1.95	0.106	0.974	0.28
s.d.	0.13	2.31	0.33	0.017	0.034	0.10
prec uncer	0.03	0.23	0.22	0.032	0.009	0.02
total uncer	0.05	0.47	0.45	0.041	0.014	0.06
net corr	0.52	1.07	0.07	0.885	1.027	0.79
Super - µm						
average	0.08	8.57	0.03	0.100	0.991	
s.d.	0.12	6.27	0.10	0.009	0.013	
prec uncer	0.05	0.38	0.16	0.018	0.005	
total uncer	0.07	1.88	0.73	0.033	0.008	
net corr	0.37	1.51	0.39	0.679	1.027	
			Asian-Modified Marine Event			
Sub - µm						
average	1.84	18.34	2.04	0.113	0.909	0.42
s.d.	0.37	2.77	0.07	0.002	0.007	0.06
prec uncer	0.14	0.44	0.09	0.007	0.007	0.01
total uncer	0.49	1.76	0.33	0.018	0.024	0.07
net corr	0.71	1.07	0.06	0.889	1.045	0.83
Super - µm						
average	0.30	25.41	0.06	0.098	0.988	
s.d.	0.17	8.14	0.05	0.004	0.004	
prec uncer	0.10	0.62	0.10	0.007	0.004	
total uncer	0.18	5.28	0.70	0.025	0.008	
net corr	0.43	1.51	0.39	0.679	1.030	
			NA-Modified Marine			
Sub - µm						
average	0.80	6.49	2.36	0.136	0.895	0.48
s.d.	0.98	5.31	0.24	0.019	0.059	0.26
prec uncer	0.06	0.27	0.15	0.018	0.009	0.03
total uncer	0.21	0.74	0.38	0.031	0.028	0.08
net corr	0.72	1.05	0.06	0.901	1.047	0.84
Super - µm						
average	0.11	7.08	0.08	0.097	0.984	
s.d.	0.16	4.51	0.13	0.009	0.023	
prec uncer	0.05	0.35	0.18	0.022	0.007	
total uncer	0.08	1.57	0.74	0.036	0.011	
net corr	0.49	1.51	0.39	0.679	1.033	
			NA Continental			
Sub - µm						
average	1.39	10.79	2.51	0.139	0.886	0.78
s.d.	0.54	5.33	0.11	0.015	0.031	0.12
prec uncer	0.10	0.33	0.12	0.011	0.008	0.04
total uncer	0.36	1.11	0.35	0.025	0.029	0.11
net corr	0.73	1.04	0.06	0.907	1.049	0.93
Super - µm						
average	0.09	3.01	0.23	0.085	0.970	
s.d.	0.12	1.92	0.47	0.013	0.037	
prec uncer	0.06	0.30	0.33	0.049	0.020	
total uncer	0.07	0.76	0.84	0.058	0.023	
net corr	0.63	1.51	0.39	0.679	1.041	

Air mass definitions are given in Table 1. Averages and standard deviations are arithmetic (see equations 5 and 6) and based on hourly data. Precision and total uncertaintics are defined in equations 7 and 8. "Net corr" shows net effect of corrections to scattering (equation 9) and absorption (equation 11) measurements.Net corr. = y/x, where y is the corrected and x the uncorrected value, except for the Ångström exponent å, where net corr = $y - x$.

Table 5. Comparison of Aerosol Light-Scattering Properties with Spring 1995 Measurements at Cape Grim, Tasmania

	Cheeka Peak		Cape Grim		Significant Difference?(*)
	Average	Precision Uncertainties	Reported	Corrected	
			Sub-μm		
σ_S, Mm^{-1}	3.34	±0.23	3.6	4.0	barely
å	1.95	±0.22	0.97	1.05	yes
b	0.106	±0.032	0.12	0.10	no
f	0.28	±0.02	0.23	0.18	yes
			Super-μm		
σ_S, Mm^{-1}	8.57	±0.38	11.8	17.8	yes
å	0.03	±0.16	-0.45	-0.06	no
b	0.100	±0.018	0.17	0.12	no

Low-RH aerosol optical data from the marine category at Cheeka Peak (Table 4) compared to the clean marine sampling periods at Cape Grim, Tasmania (40.7°S, 144.6°E), during the 1-month Aerosol Characterization Experiment, November 15 to December 15, 1995 [*Carrico et al.*, 1998]. Cape Grim scattering measurements are corrected (column 5) according to the scheme presented herein. See Table 6 for σ_a data from Cape Grim, obtained during a different campaign.

*Different if uncertainty ranges do not overlap. Assessed using corrected Cape Grim data and assuming its precision uncertainty is identical to the Cheeka Peak data.

umn 5). In addition, we assume that precision uncertainties are identical between the two data sets. Differences between the two stations are assessed (column 6) by testing whether or not the precision uncertainty ranges overlap.

At both stations, light scattering during marine sampling is dominated by super-μm (sea salt) particles. Super-μm scattering is significantly higher at Cape Grim (18 versus 9 Mm^{-1}), and the sub-μm fraction of scattering *f* is significantly smaller (0.18 versus 0.28). These differences are probably associated with a sampling site that is closer in elevation (104 versus 480 m) and in horizontal distance (0.1 versus 3 km) to the ocean surface. Support for this explanation comes from shipboard light scattering data during ACE 1 [*Quinn et al.*, 1998] which shows a sub-μm scattering fraction (after applying the same correction scheme) of 0.11 (data obtained from D. Coffman, personal communication, 1998). The substantially lower value of sub-μm å at Cape Grim (1.05 versus 1.95) indicates that the sub-μm tail of the seasalt size distribution is also enhanced at Cape Grim relative to Cheeka Peak. Sub-μm å is a sensitive indicator of the distribution of sub-μm particle mass. Accumulation mode particles (with most mass in the 0.1 to 0.4μm diameter range) are associated with å values in the 2.0 to 2.5 range, while a sub-μm sea-salt tail (with most mass just below 1 μm diameter) is associated with å values in the 0.0 to 0.5 range. Despite the large difference in the size distribution of sub-μm mass, as evidenced by the å values, the backscatter fractions for sub-μm particles are indistinguishable. This is not surprising. Whereas the Ångström exponent changes monotonically with sub-μm particle size, the backscatter fraction (at 550 nm wavelength) manifests a local minimum at about 0.5 μm diameter.

Light absorption data from a variety of marine and coastal measurements (including Cape Grim) are compared in Table 6. As indicated by asterisks, most of these data were originally reported in terms of mass concentration of "black carbon" (BC). We note, however, that BC was actually detected in each of these cases by optical, filter-based, light attenuation methods, similar to our measurement of σ_a. It is not clear whether such measurements bear a closer relationship to the ambient, low-RH light absorption coefficient or to the ambient mass concentration of BC. Recent optical calibrations [*Horvath*, 1997; *Bond et al.*, 1999] have shown the relationship with ambient, low-RH light absorption is bounded well within a factor of 2, while studies addressing the latter relationship [*Petzold et al.*, 1997; *Liousse et al.*, 1993] have indicated uncertainties of a factor of 2-4. For these reasons, we convert all reported BC mass concentrations to σ_a, using a conversion factor of 10 m^2 g^{-1}. Owing to the lack of actual calibrations in terms of σ_a and the lack of corrections for response to particle scattering [*Heintzenberg et al.*, 1997], the values of σ_a listed in Table 6 from stations other than Cheeka Peak should be considered uncertain by at least a factor of 2. For that reason, only ranges will be compared. We retain the term BC in the discussion below to refer to the portion of sub-μm particulate mass that is light absorbing.

Despite large uncertainties, the comparisons are quite useful. Marine values of sub-μm σ_a are seen to vary by 2-3 orders of magnitude, from "clean" values generally below 0.1 Mm^{-1} to "perturbed" values in the 1-10 Mm^{-1} range. This reflects a combination of factors: (1) the exclusive production of BC by combustion and thus the absence of sources over the ocean, (2) the sporadic nature of atmospheric transport and removal of BC, and (3) the sporadic nature of at least one major source of BC: biomass burning. This variability imposes difficulties on modeling the atmospheric cycle of BC and its radiative effects, as well as on the validation of models from observations. It is possible, for instance, that global averages are dominated by a relatively small number of high concentration "events" (i.e., highly confined in space and time). Somewhat similar variability in carbon monoxide con-

Table 6. Comparison of Sub-μm Aerosol Light Absorption With Other Surface-Based Marine and Coastal Measurements

Location	Marine		Continental	Reference	Notes
	Clean, Mm^{-1}	Perturbed, Mm^{-1}	Sector, Mm^{-1}		
East China Sea		1.0 - 10.0		P94	1*
Tropical Pacific	0.14			A84	2*
Midlatitude western Pacific	0.02 - 0.09	0.75 - 13.0		Cl89	3
Midlatitude SH	0.01 - 0.06			HB90	4*
Midlatitude eastern Atlantic	0.17 - 0.45		0.6 - 3.8	Co97	5*
Midlatitude eastern Pacific	0.09 ± 0.13	1.8 ± 0.4	1.4 ± 0.5	this work	6

Low-RH aerosol light absorption at 550 nm, σ_a, at a variety of marine and coastal surface-based sites. References are as follows: A84, *Andreae et al.* [1984]; Cl89, *Clarke* [1989]; Co97, *Cooke et al.* [1997]; HB90, *Heintzenberg and Bigg* [1990]; P94, *Parungo et al.* [1994]. Notes: (1) shipboard measurements downwind of Chinese industrial emissions; (2) Shipboard measurements (n=11) during July-August 1982 between Equador and Hawaii; (3) clean: shipboard measurements (n=35) during May-June 1982 in central North Pacific; Perturbed: shipboard measurements (n=15) during May-June, 1987 in NW Pacific coincident with extensive Asian forest fires; (4) coastal measurements (Cape Grim, Tasmania, 40.7°S, 144.6°E, 104 m); spring only (September/October/November); one standard deviation range for 7 years of measurements over 1982-1990, clean Marine sector only; (5) coastal measurements (Mace Head, Ireland, 43.3°N, 9.9°W, 40 m); spring only (March/April/May); range of listed monthly geometric means for 7 years of measurements over 1989-1996 for clean marine and continental wind sectors. Clean marine data are screened to exclude hourly averaged values of $\sigma_a > 0.75$ Mm^{-1} (BC > 75 ng m^{-3}); (6) coastal measurements (Cheeka Peak, Washington, 48°N, 125°W, 480 m) in March-April 1997; average plus or minus one standard deviation for marine, Asian, and continental air masses, as defined in Table 1.

*Detected optically but reported as soot, elemental, or black carbon mass (μg m^{-3}). Converted here to σ_a using 10 m^2 g^{-1}.

centrations was observed by *Jaffe et al.* [1997], who showed that the advection of polluted air masses over the North Pacific is often highly episodic, rather than causing a well-mixed general increase.

In addition to marine values, Table 6 shows values of sub-μm σ_a at two coastal stations, Cheeka Peak and Mace Head, Ireland, during continental sector winds. The ranges (roughly 1-2 Mm^{-1}) are similar to each other as well as to the perturbed marine levels.

4.3. Estimated optical properties of non-sea-salt aerosol at high RH

For practical reasons, the measurements reported herein were made at low RH and for the existing mixture of natural and anthropogenic aerosol constituents. However, it is the anthropogenic portion of the aerosol at ambient RH that is associated with anthropogenic climate forcing. Table 7 presents estimated optical properties of non-sea-salt aerosol (used as a preliminary proxy for anthropogenic aerosol) at low and high RH. Uncertainties in the original measurements and in the calculation scheme described below are propagated in order to assess the sources of uncertainty in climate forcing.

The most obvious step toward evaluating the effects of anthropogenic aerosols at Cheeka Peak is to remove the effects of sea-salt. We do this by assuming that the super-μm aerosol is entirely sea-salt (which is reasonable given the very high ω values in all cases) and that there is a constant ratio of sub-μm to super-μm scattering caused by sea-salt. We assess this ratio as 0.20±0.05, based on the measured, marine-sector ratio of sub-μm to super-μm scattering (0.28/(1.00-0.28); see Table 4) and on prior measurements at Cheeka Peak [*Quinn et al.*, 1995] indicating that about 50% of the sub-μm scattering is due to sea salt for marine samples. Using this result, we estimate sub-μm, non-sea-salt scattering for each air mass category by subtracting from the measured value an amount equal to 0.20±0.05 times super-μm scattering. (This procedure is used for both total scatter and backscatter.)

The remaining, non-sea-salt aerosol is then hydrated to approximately 80% RH based on the RH-dependent light scattering measurements at the polluted continental station of Bondville, Illinois. Springtime measurements at that station indicate that an increase in RH from 40% to 80% is associated with an increase in sub-μm σ_s by a factor of 1.7±0.3 and in sub-μm σ_{bs} by a factor of 1.2±0.1 [*Shrestha*, 1996]. Lacking empirical data, we assume that the hydration effect on absorption σ_a is small - a factor of 1.1 ± 0.1 is used.

The steps outlined above are sufficient for estimating the key aerosol properties of backscatter ratio b and single scattering albedo ω, along with their uncertainties. Results are shown in Table 7. Taking the marine air mass category as an example, the average value of b as measured at low RH is 0.106 with an uncertainty of 0.041, while the estimated value of b for non-sea-salt aerosol at high RH is 0.079 with an uncertainty of 0.046. For ω, the measured, low-RH value and uncertainty are 0.974 and 0.014, while the estimated non-sea-salt, high-RH value and uncertainty are 0.965 and 0.043. In general, the dominant source of uncertainty for b is associated with the low-RH measurements, while for ω, large sources of additional uncertainty are associated with both the non-sea-salt and the hydration calculations. This implies that improved measurements of low-RH aerosol backscatter would be highly

Table 7. Estimated Optical Properties of Non-Sea-Salt Component of Sub-μm Aerosol at Low and High Relative Humidity (RH)

	b		ω		RFE (W m^{-2})	
	Average	Total Uncertainties	Average	Total Uncertainties	Average	Relative Uncertainties, %
Marine (Excluding Asian Event)						
Low RH	0.106	0.041	0.974	0.014	-32.0	21
Low-RH non-sea-salt	0.112	0.042	0.946	0.025	-31.5	20
High-RH non-sea-salt	0.079	0.046	0.965	0.043	-26.9	31
Asian Event						
Low RH	0.113	0.018	0.909	0.024	-29.3	9
Low-RH non-sea-salt	0.119	0.018	0.874	0.031	-28.3	10
High-RH non-sea-salt	0.084	0.026	0.914	0.064	-25.2	19
Modified Marine						
Low RH	0.136	0.031	0.895	0.028	-31.6	13
Low-RH non-sea-salt	0.147	0.032	0.864	0.038	-31.3	13
High-RH non-sea-salt	0.104	0.040	0.908	0.065	-28.0	23
Continental						
low-RH	0.139	0.025	0.886	0.029	-31.3	10
low-RH non-seasalt	0.142	0.025	0.875	0.036	-31.4	11
high-RH non-seasalt	0.100	0.032	0.916	0.053	-27.9	19

Backscatter fraction b and single scattering albedo ω from measurements ("low RH", see Table 4) and from calculations to remove sea-salt scattering ("low-RH non-sea-salt") and hydrate the remaining aerosol to about 80% RH ("high-RH non-sea-salt"). Final two columns show radiative forcing efficiency [*Ogren et al.*, 1999] and the relative uncertainty in this quantity due to the listed uncertainties in b and ω. Sub-μm sea-salt scattering is assumed to equal 20±5% of super-μm scattering. Total scatter and backscatter are assumed to increase at high RH by factors of 1.7±0.3 and 1.2±0.1, respectively, based on measurements at a polluted site in Bondville, Illinois [*Shrestha*, 1996]. Lacking empirical data, we assume the hydration effect on absorption is small (1.1±0.1). The forcing estimate uses a surface albedo of 0.07, appropriate to the ocean. See text for other calculation details.

valuable. This is an approachable, signal-to-noise issue for nephelometer measurements. On the other hand, improved measurements of low-RH single scattering albedo would eventually produce diminishing returns as long as uncertainties in anthropogenic aerosol fraction and hydration effects on both scattering and absorption remain high. (We note, however, that our low-RH uncertainty evaluation hinges upon the estimated ±20% uncertainty in the PSAP calibration, which has not been experimentally confirmed. Moreover, the measurements and discussion herein apply to 550 nm wavelength; additional, and potentially large uncertainty, is associated with the wavelength dependence of ω.)

The final two columns in Table 7 combine the values of b and ω into a single radiative forcing efficiency (RFE) parameter [*Ogren et al.*, 1999], defined herein as

$$RFE = SD(1-A_c)T_{at}^2(1-R_s)^2\left[2R_s\frac{1-\omega}{(1-R_s)^2}-\beta(b)\omega\right] \quad (14)$$

where RFE and S have units of W m^{-2}, S is the solar constant (set to 1370), D is the daylight fraction (set to 0.5), A_c is the fractional cloud cover (set to 0.6), T_{at} is the atmospheric transmissivity (set to 0.76), R_s is the surface albedo (set to 0.07, appropriate to the ocean), and $\beta(b)$ is the average upscatter fraction (i.e., the fraction of scattered sunlight that is scattered into the upward hemisphere, away from the Earth), which we parameterize as a simple function of b. (We use $\beta = 0.082 + 1.85b - 2.97b^2$, which closely approximates the relationship for a Henyey-Greenstein phase function.) The RFE is derived from the aerosol climate forcing equation of *Haywood and Shine* [1995, equation (3)] by dividing both sides by aerosol optical depth. It represents the normalized, top-of-atmosphere, shortwave flux change (increased absorption minus increased upscatter) caused by a globally uniform, optically thin aerosol layer in the lower troposphere. Owing to a number of simplifying assumptions (for example, neglect of the spectral dependence of aerosol and atmospheric optical properties, here studied only at 550 nm), equation (14) provides nothing more than a zero-order estimate of radiative flux changes. Despite this limitation, the RFE parameter is valuable in that it allows us to assess how uncertainties in b and ω propagate into uncertainties in direct climate forcing.

In terms of this quantity, there is remarkably little variation among air mass types, reflecting the fact that the variations in b and ω tend to be compensating. Note that aerosol hydration causes a decrease in the magnitude of RFE; this is due to the decrease in backscatter fraction as particle size increases,

which outweighs the increase in ω. (The increase in total extinction with hydration has no effect, since RFE is the forcing per unit optical depth.) The estimated uncertainty at high RH is of the order of ±20% for all but the marine air mass category (which has a much higher relative uncertainty in ω). This value represents the uncertainty in climate forcing associated with uncertainties in the measured and derived intensive aerosol optical properties reported herein. It is an encouraging result because it implies that measurement-based approaches have the potential to dramatically improve the accuracy of current estimates of direct climate forcing by anthropogenic aerosols. (This accuracy is currently estimated at a factor of 2-3.) To achieve this, however, will require adequate sampling of aerosol spatial and temporal variations. For intensive aerosol properties (which appear to be relatively constant), an expanded network of monitoring stations combined with systematic airborne measurements should suffice. For the highly variable aerosol extensive properties, only satellites would seem to offer the needed spatial and temporal coverage.

5. Conclusions and Future Work

Aerosol optical properties relevant to direct climate forcing were investigated during a 2-month campaign at a midlatitude, Pacific coastal station at Cheeka Peak, Washington (48°N, 125°W, 480 m). Measurement and data reduction methods focused on backscatter ratio and single-scattering albedo at low-RH and 550 nm wavelength and on a rigorous determination of the uncertainty of optical properties. Data were separated into three air mass categories based on local winds and calculated back trajectories. These categories are marine, North-American-modified marine, and North-American continental. Because of its highly distinct properties, a single episode, dubbed the "Asian-modified marine Event," was extracted from the marine category for separate analysis.

Primary measurements were light scattering by nephelometry (TSI model 3563) and light absorption by differential transmission through a filter (Radiance Research model PSAP). Inertial impactors were used to separately analyze the contributions of sub-μm and super-μm particles (low-RH, aerodynamic diameter). Both scattering and absorption data were corrected for known instrumental nonidealities: angular nonidealities in the case of the nephelometer (following *Anderson and Ogren* [1998]) and response to light scattering in the case of the PSAP (following *Bond et al.* [1999]). The light scattering correction was partially validated by measurements of sea salt aerosol (which is nonabsorbing) during this campaign.

The main source of uncertainty in single scattering albedo (ω) measurements, namely, the measurement of light absorption, was addressed by the deployment of three, identical PSAPs and by relying on a recent calibration of this device referenced to the ambient absorption coefficient, determined as extinction minus scattering [*Bond et al.*, 1999]. Precision uncertainties were determined by analyzing the discrepancies among the three PSAPs. Averaged over the campaign, unit-to-unit discrepancies were found to be within 6%, while the average noise level for 24-min sample times was 0.18 Mm^{-1} (both to 95% confidence). Significant unit-to-unit differences in noise were found. We recommend therefore that this quantity be determined for individual PSAP units, via measurements of filtered air, rather than adopting the value determined herein.

Uncertainties stemming from instrumental noise, drift, calibration, and correction factors were assessed and propagated. Two summary uncertainty values are reported: precision uncertainty and total uncertainty. Precision uncertainty allows comparison among measurements using identical methods but separated in time or space. Using this criterion, we find significant differences in the optical properties among air mass categories at Cheeka Peak but considerable similarities between the marine aerosol at Cheeka Peak and that at the Southern Hemisphere coastal station of Cape Grim, Tasmania. Total uncertainty (or overall accuracy) allows for comparison with alternate measurement methods and indicates how tightly constrained the optical properties are when used as inputs to climate models.

Marine aerosol over the midlatitude eastern Pacific is found to be weakly absorbing for the sub-μm component and virtually nonabsorbing for the super-μm component. Excluding the Asian-modified marine event, the means and 95% confidence limits of ω for sub- and super-μm particles are 0.97+/-0.01 and 0.99+/-0.01, respectively. During the Asian event, sub-μm extinction increased from 3 to 20 Mm^{-1}, and sub-μm ω decreased from 0.97 to 0.91. In general, continental influence, as indicated by trends over the air mass categories, tends to raise the backscatter ratio b and lower ω. In terms of radiative forcing efficiency, these are largely compensating effects.

We find NO_x to be an extremely useful tracer of nearby combustion sources. As shown by the Asian event, the combination of high σ_a and low NO_x is a powerful indicator of long-range-transported, combustion-derived aerosol. The traditional continental tracer, Rn, is much less decisive owing to its longer atmospheric residence time (half-life of 3.8 days versus about 1 day for NO_x).

The Asian-modified marine event indicates that pollution from that continent is capable of modifying the aerosol optical properties over large regions of the Pacific. While the full chemical composition of this aerosol was not determined, elemental analysis showed that both sea salt and non-sea-salt sulfate were major components and that mineral dust was not. Combined with the high levels of light absorption (indicative of combustion), we conclude that this was an episode of Asian industrial pollution mixed with unusually high levels of wind-generated seasalt. The nature and implications of this episode are discussed further by *Jaffe et al.* [1999].

A comparison of our light absorption measurements σ_a to previous coastal and marine boundary-layer measurements confirms the range of values found by others and the highly variable nature of this quantity. At least a factor-of-100 variation exists between "clean" and "perturbed" conditions, such that overall average effects may be heavily influenced by the frequency and extent of "perturbed" cases.

In order to estimate how the measurement uncertainties reported here would propagate to climate forcing uncertainty, a simple calculation scheme was used to derive the optical properties of sub-μm, non-sea-salt aerosol at both low and high RH. For the backscatter ratio b, the dominant source of uncertainty is associated with the low-RH measurements, while for both ω and radiative forcing efficiency [*Ogren et al.*, 1999], large sources of additional uncertainty are associated with aerosol hydration. Thus improved measurements of

b would be valuable and could be achieved, according to our uncertainty analysis by reducing the offset uncertainty in the backscatter coefficient. This, in turn, would require more frequent filtered-air measurements than were used herein. For ω, on the other hand, improved measurements at low RH will be valuable only if coupled with an improved ability to measure the effects of aerosol hydration. (The wavelength dependence of ω is an additional area, not analyzed here, where improved measurement capabilities are needed.) Overall, the approach demonstrated herein is shown to offer a strong constraint on direct climate forcing. Uncertainties in forcing stemming from the optical properties so determined are 10-30%.

Acknowledgments. This work was supported by the National Oceanic and Atmospheric Administration (JISAO agreement NA37RJ0198, contribution 593) and by the National Science Foundation (grant ATM-9320871).

References

Anderson, T. L., and J. A. Ogren, Determining aerosol radiative properties using the TSI 3563 integrating nephelometer, *Aerosol Sci. Technol., 29*, 57-69, 1998.

Anderson, T. L., et al., Performance characteristics of a high-sensitivity, three-wavelength total scatter/backscatter nephelometer, *J. Atmos. Oceanic Technol., 13*, 967-986, 1996.

Andreae, M. O., T. W. Andreae, R. J. Ferek, and H. Raemdonck, Long-range transport of soot carbon in the marine atmosphere, *Sci. Total Environ., 36*, 73-80, 1984.

Beine, H. J., D. J. Jaffe, J. A. Herring, J. A. Kelley, T. Krognes, and F. Stordal, High latitude springtime photochemistry, I, NO_x, PAN, and ozone relationships, *J. Atmos. Chem., 27*, 127-153, 1997.

Berner, A., C. H. Lurzer, F. Pohl, O. Preining, and P. Wagner, The size distribution of the urban aerosol in Vienna, *Sci. Total Environ., 13*, 245-261, 1979.

Bond, T., T. L. Anderson, and D. Campbell, Calibration and intercomparison of filter-based measurements of visible light absorption by particles, *Aerosol Sci. Technol.*, in press, 1999.

Cahill, T. A., Composition analysis of atmospheric aerosols, *Particle-Induced X-Ray Emission Spectrometry*, edited by S. A. E. Johansson, pp. 237-311, John Wiley, New York, 1995.

Carrico, C. M., M. J. Rood, and J. A. Ogren, Aerosol light scattering properties at Cape Grim, Tasmania, during the First Aerosol Characterization Experiment (ACE 1), *J. Geophys. Res., 103*, 16565-16574, 1998.

Clarke, A. D., Aerosol light absorption by soot in remote environments, *Aerosol Sci. Technol., 10*, 161-171, 1989.

Cooke, W. F., S. G. Jennings, and T. G. Spain, Black carbon measurements at Mace Head, 1989-1996, *J. Geophys. Res., 102*, 25339-25346, 1997.

Hansen, J., M. Sato, and R. Ruedy, Radiative forcing and climate change, *J. Geophys. Res., 102*, 6831-6864, 1997.

Harris, J. M., and J. D. W. Kahl, Analysis of 10-day isentropic flow patterns for Barrow, Alaska: 1985-1992, *J. Geophys. Res., 99*, 25845-25855, 1994.

Haywood, J. M., and K. P. Shine, The effect of anthropogenic sulfate and soot aerosol on the clear-sky planetary radiation budget, *Geophys. Res. Lett., 22*, 603-606, 1995.

Heintzenberg, J., and E. K. Bigg, Tropospheric transport of trace substances in the southern hemisphere, *Tellus, Ser. B, 42*, 355-363, 1990.

Heintzenberg, J., R. J. Charlson, A. D. Clarke, C. Liousse, V. Ramaswamy, K. P. Shine, M. Wendisch, and G. Helas, Measurement and modeling of aerosol single-scattering albedo: Progress, problems and prospects, *Contrib. Atmos. Phys., 70*, 249-263, 1997.

Horvath, H., Experimental calibration for aerosol light absorption measurements using the integrating plate method - Summary of the data, *J. Aerosol Sci., 28*, 1149-1161, 1997.

Jaffe, D., A. Mahura, J. Kelley, J. Atkins, P. C. Novelli, and J. Merrill, Impact of Asian emissions on the remote North Pacific atmosphere: Interpretation of CO data from Shemya, Guam, Midway, and Mauna Loa, *J. Geophys. Res., 102*, 28627-28635, 1997.

Jaffe, D. A., et al., Transport of Asian air pollution to North America, *Geophys. Res. Lett.*, in press, 1999.

Liousse, C., H. Cachier, and S. G. Jennings, Optical and thermal measurements of black carbon aerosol content in different environments: Variation of the specific attenuation cross section, sigma (σ), *Atmos. Environ., Part A, 27*, 1203-1211, 1993.

Liousse, C., J. E. Penner, C. Chuang, J. J. Walton, H. Eddleman, and H. Cachier, A global three-dimensional model study of carbonaceous aerosols, *J. Geophys. Res., 101*, 19411-19432, 1996.

McInnes, L. M., P. K. Quinn, D. S. Covert, and T. L. Anderson, Gravimetric analysis, ionic composition, and associated water mass of the marine aerosol, *Atmos. Environ., 30*, 869-884, 1996.

Ogren, J. A., M. H. Bergin, R. J. Charlson, D. S. Covert, T. L. Anderson, and M. J. Rood, Measurements of aerosol single scattering albedo: implication of its observed variability on estimates of aerosol radiative forcing, paper presented at *ALPS99 Symposium*, Centre National d'Etudes Spatiales, Meribel, France, Jan., 1999.

Parungo, F., C. Nagamoto, M.-Y. Zhou, A. D. A. Hansen, and J. Harris, Aeolian transport of aerosol black carbon from China to the ocean, *Atmos. Environ., 28*, 3251-3260, 1994.

Petzold, A., C. Kopp, and R. Niessner, The dependence of the specific attenuation cross section on black carbon mass fraction and particle size, *Atmos. Environ., 31*, 661-672, 1997.

Quinn, P. K., S. Marshall, T. S. Bates, D. S. Covert, and V. N. Kapustin, Comparison of measured and calculated aerosol properties relevant to the direct radiative forcing of tropospheric sulfate aerosol on climate, *J. Geophys. Res., 100*, 8977-8991, 1995.

Quinn, P. K., D. J. Coffman, V. N. Kapustin, T. S. Bates, and D. S. Covert, Aerosol optical properties in the marine boundary layer during the First Aerosol Characterization Experiment (ACE 1) and the underlying chemical and physical aerosol properties, *J. Geophys. Res., 103*, 16547-16563, 1998.

Raabe, O. G., D. A. Braaten, R. L. Axelbaum, S. V. Teague, and T. A. Cahill, Calibration studies of the drum impactor, *J. Aerosol Sci., 19*, 183-195, 1988.

Rosen, J. M., R. G. Pinnick, and D. M. Garvey, Measurement of extinction-to-backscatter ratio for near-surface aerosols, *J. Geophys. Res., 102*, 6017-6024, 1997.

Shrestha, R. P., Light scattering by aerosol particles at an anthropogenically perturbed, midlatitude, continental site and its dependence on particle mass, composition, and air mass trajectories, M.S. thesis, 130 pp., Univ. of Ill. at Urbana-Champaign, 1996.

Whittlestone, S., S. D. Schery, and Y. Li, Thoron and radon fluxes from the island of Hawaii, *J. Geophys. Res., 101*, 14787-14794, 1996.

T. L. Anderson (corresponding author), Joint Institute for the Study of the Atmosphere and Ocean, Box 351640, University of Washington, Seattle, WA 98195-1640. (tadand@u.washington.edu)

D. S. Covert, Department of Atmospheric Sciences, Box 351640, University of Washington, Seattle, WA 98195-1640.

J. M. Harris and J. A. Ogren, Climate Monitoring and Diagnostics Laboratory, NOAA, Boulder, CO 80803.

D. J. Jaffe, Department of Science, Technology, and the Environment, University of Washington, Bothell, WA 98021.

K. D. Perry, Crocker Nuclear Laboratory, University of California, Davis, CA 95616.

B. E. Trost, Department of Geophysics, University of Alaska, Fairbanks, AK 99701.

J. D. Wheeler, College of Oceanic and Atmospheric Sciences, Oregon State University, Corvallis, OR 97331.

(Received October 16, 1998; revised March 4, 1999;
accepted March 8, 1999.)